Title

Fluorescent toxins as ion channel activity sensors

Permalink

Authors

Stewart, Robert

Cohen, Bruce E

Sack, Jon T

Publication Date

2021

DOI

Peer reviewed

Fluorescent Toxins as Ion Channel Activity Sensors

Authors

Robert Stewart[1], Bruce E. Cohen[2,3]*, Jon T. Sack[1,4]*

[1]Department of Physiology & Membrane Biology

[4]Department of Anesthesiology & Pain Medicine

University of California, Davis, CA 95616

[2]The Molecular Foundry

[3]Division of Molecular Biophysics & Integrated Bioimaging

Lawrence Berkeley National Laboratory, Berkeley, CA 94720

*Correspondence to jsack@ucdavis.edu, becohen@lbl.gov

Fluorescent Toxins as Ion Channel Activity Sensors

Contents

Abstract

Voltage gated ion channels (VGICs) shape the electrical character of cells by undergoing structural changes in response to membrane depolarization. High-resolution techniques have provided a wealth of data on individual VGIC structures, but the conformational changes of endogenous channels in live cell membranes have remained unexplored. Here, we describe methods for imaging structural changes of voltage-gated K^+ channels in living cells, using peptidyl toxins labeled with fluorophores that report specific protein conformations. These Endogenous Voltage-sensor Activity Probes (EVAPs) enable study of both VGIC allostery and function in the context of endogenous live-cell membranes under different physiological states. In this chapter we describe methods for the synthesis, imaging, and analysis of, dynamic EVAPs, which can report K^+ channel activity in complex tissue preparations via 2-photon excitation microscopy, and environment-sensitive EVAPs, which report voltage-dependent conformational changes at the VGIC-toxin interface. The methods here present the utility of current EVAPs and lay the groundwork for the development of other probes that act by similar mechanisms. EVAPs can be correlated with electrophysiology, offering insight into the molecular details of endogenous channel function and allostery in live cells. This enables investigation of conformational changes of channels in their native, functional states, putting structures and models into a context of live-cell membranes. The expansive array of state-dependent ligands and optical probes should enable probes more generally for investigating the molecular motions of endogenous proteins.

1. Introduction

Structural changes in proteins are at the heart of all cellular processes. Techniques that measure protein conformational change are fundamental to understanding how these molecular machines produce the emergence of cell physiology. While X-ray crystallography and single particle cryo-EM are able to decode full channel structures with angstrom resolution, there are few techniques able to describe the dynamics of endogenous proteins *in vivo*. To address these limitations, additional probes and methods are required to investigate live-cell protein dynamics. The probes we discuss here report on specific voltage-sensitive conformations of K^+ channels. The approaches presented here describe two types of Endogenous Voltage-sensor Activity Probes (EVAPs) and their unique methods for imaging conformational changes of voltage-gated K^+ channels.

Activity probes may be synthesized from ligands that are specific for individual ion channels and that preferentially bind to specific channel conformations. Venomous species commonly target ion channels with peptidyl gating-modifying toxins that preferentially bind to specific channel conformations (Catterall et al., 2007). These conformation-selective ligands are ideal scaffolds for synthesizing EVAP probes. Here we describe methods for deploying EVAPs that are variants of guangxitoxin-1E, or GxTX, a lipophilic cystine-knot peptide from the Chinese hissing bronze wolf tarantula *C. guangxiensis* (Herrington et al., 2006). GxTX targets the resting conformation of the voltage sensor domain (VSD) of the voltage gated K^+ channel subunit Kv2.1, with at least 5400-fold greater affinity than activated conformations (Tilley et al., 2019). Synthetic analogs of GxTX have been functionalized with optical probes and preferentially bind to the resting VSD

conformation of Kv2.1 channels in cells and tissue, and dissociate when channels are voltage activated (Fig 1 and 2) (Tilley et al., 2014).

[Insert Figure 1 here]

Kv2 proteins are members of the voltage-gated cation channel superfamily, whose VSDs are comprised of bundles of four transmembrane helices termed S1-S4 (Long et al., 2005). The VSD S4 helix contains positively charged arginine and lysine residues, which respond to voltage changes by moving through the transmembrane electric field to create measurable gating charges (Aggarwal & MacKinnon, 1996; Islas & Sigworth, 1999; Seoh et al., 1996). When VSDs encounter a transmembrane voltage that is more negative on the inside of the cell membrane, voltage sensors are biased towards resting conformations, or down states, in which gating charges reside closer to the cell interior. When the membrane voltage becomes more positive, these gating charges translate towards the extracellular side of the membrane, and voltage sensors are progressively biased towards up states, in a process of voltage activation (Armstrong & Bezanilla, 1973; Tao et al., 2010; Xu et al., 2019; Zagotta et al., 1994).

To image where the voltage sensors of Kv2 proteins adopt a specific resting conformation in tissue, we exploit the conformation-selective binding of GxTX variants functionalized with optical probes to report Kv2 conformational changes (Fletcher-Taylor et al., 2020; Thapa et al., 2021; Tilley et al., 2014). Given the large number of conformation-specific ion channel toxins (Ahuja et al., 2015; Catterall et al., 2007; Dockendorff et al., 2018; McCormack et al., 2013; McDonough et al., 1997; Peretz et al., 2010; Sack et al., 2004; Schmalhofer et al., 2008; Swartz, 2007; Zhang et al., 2018), this approach may be exploited against numerous channels.

Here we provide protocols for two types of probes, dynamic EVAPs which report channel activity in complex tissue preparations, and environment-sensitive EVAPs which report conformational changes at the VSD-toxin interface.

Dynamic EVAPs label Kv2 proteins on cell surfaces in response to voltage stimulation. For these probes, a statistical thermodynamic model can be used to relate the conformational changes of Kv2 voltage sensors to labeling intensity (Thapa et al., 2021). We have generated dynamic EVAPs which are compatible with 2-photon excitation imaging to investigate Kv2 proteins deep within tissues (Thapa et al., 2021). Environment-sensitive EVAPs have a fluorophore that interacts closely with the channel. The fluorophore is an environment-sensitive dye, whose emission is responsive to changes in the surrounding polarity (Fletcher-Taylor et al., 2020). By using voltage clamp spectroscopy to collect emission spectra as a function of membrane potential, conformational changes at the toxin-channel interface associated with early gating charge transitions can be measured. Environment-sensitive probes enable study of channel allostery with correlated electrophysiology, putting channel structures and models into a context of live-cell membranes and physiological states.

2. Conformation-Sensitive Ligands to Image Structural Changes

The molecular targeting, conformation selectivity, and spatial precision of fluorescence from EVAPs enable identification of where in tissue the conformational status of ion channels change. We discuss the potential utility and limitations of the EVAP mechanism.

2.1 Unique capabilities of EVAPs

EVAPs are the only imaging method we are aware of for measuring voltage-sensitive conformational changes of a specific, endogenous protein. An advantage of measuring voltage dependent conformation changes with EVAPs over conventional electrophysiological techniques is EVAP fluorescence allows imaging of channel activation at specific, subcellular anatomical locations. With the dynamic EVAP, GxTX-594, we noted on CA1 hippocampal neurons that the majority of detectable Kv2 protein at discrete individual clusters were voltage sensitive (Thapa et al., 2021). While it may not sound surprising to find that the VSDs of ion channel proteins are voltage sensitive, this is not always the case. For example, some gating charge of the L-type Ca^{2+} channel Cav1.2 can be immobilized until it is bound by an intracellular protein (Turner et al., 2020).

2.2 Probe signal versus perturbation of cell physiology

Ligands that bind selectively to a specific protein conformation alter protein activity (Lewis, 1925). GxTX-based probes inhibit the Kv2 proteins they label by stabilizing the resting conformation of Kv2 voltage sensors such that the complex does not activate in the physiological voltage range (Fletcher-Taylor et al., 2020; Tilley et al., 2019). Thus, GxTX depletes the population of Kv2 proteins responding normally to physiological stimuli. If this depletion is a

concern, one solution is to lower the EVAP concentration (Fig 2) (Tilley et al. 2014). The trade off in lowering concentration is diminished signal to noise limiting ability to detect physiological changes. Brighter EVAPs (Mann et al. 2018) can mitigate this issue to some degree. Higher EVAP concentrations that alter cell physiology may provide meaningful data if analyzed by EVAP models that extract the behavior of unlabeled Kv2 proteins (Thapa et al., 2021). This analysis uses the amplitude of fluorescence change to calculate the $V_{1/2}$ of unlabeled Kv2 channels, enabling measurements of the conformational state of Kv2 channels by imaging.

[Insert Figure 2 here]

2.3 Dynamic EVAPs

Measurements of dynamic labeling by a conformation-selective probe such as an EVAP can enable deduction of how unlabeled proteins behave. This is perhaps counterintuitive because only bound proteins generate optical signals. Our approach to reveal the behavior of unlabeled proteins is analogous to calcium imaging experiments, which have been spectacularly informative about physiological calcium signaling (Yang & Yuste, 2017). During Ca^{2+} imaging experiments, no optical signals originate from the physiologically relevant free Ca^{2+}, only from Ca^{2+} that is chelated by a dye. Fluorescence Ca^{2+} imaging is so informative because fluorescence from Ca^{2+}-bound dyes is deconvolved using the statistical thermodynamics of Ca^{2+} binding to calculate free Ca^{2+} (Adams, 2010). Similarly, fluorescence from an EVAP is deconvolved using the statistical thermodynamics of binding to determine the conformational state of unbound channels (Fig 3).

[Insert Figure 3 here]

The thermodynamics of the ensemble of free EVAP, labeled and unlabeled ion channel proteins reduce to a simple interpretation: a change in EVAP labeling indicates conformational change has occurred in the unlabeled channels. Membrane-localized fluorescence decreases when EVAP-labeled voltage sensors become voltage-activated and EVAPs dissociate, diffusing into the surrounding solution (Figs 1 and 2). Membrane-localized fluorescence increases when unlabeled voltage sensors return to resting conformations (Fig 4). Thus dynamic EVAPs act by binding and dissociating in response to conformational changes. This mechanism of dynamic EVAPs requires that they respond more slowly than channels change conformation. Thus, dynamic EVAPs would be hard-pressed to reveal kinetic information on the time scale of action potentials. The kinetics of the GxTX-based dynamic EVAPs described here are limited to measuring changes in Kv2 activity on a time scale of tens of seconds. This slow response time limits measurements to the probability, averaged over time, that voltage sensors are resting or active (Thapa et al., 2021).

An additional consideration important for dynamic EVAPs is access of EVAPs to their target channels. Any ligand-based approach requires access of the ligand to the target protein, and these dynamics can be altered by the particular spatial arrangements within cells and tissue. For example, fluorescence from the dynamic EVAP GxTX-594, responds to voltage changes more slowly at the center of the glass-adhered surface of CHO cells relative to more peripheral regions, which have better access to the bath solution (Fig 4). The different EVAP dynamics in a restricted space is significant because cells in tissue are crowded together. For example, the space extracellular to Kv2.1 channel clusters is restricted in many neurons. The Kv2 channel

clusters in the plasma membrane of hippocampal and cortical interneurons are tightly associated with astrocytic end feet and the cleft between these two membranes is a few nanometers wide (Du et al., 1998). Interpretation should consider the limitations of using EVAP probes in restricted spaces; most notably the finding that labeling dynamics are more dramatically affected than unlabeling dynamics (Fig 4).

[Insert Figure 4 here]

2.4 Environment-Sensitive EVAPs

Environment-sensitive fluorophores are designed with asymmetric structures that respond to the polarity of their immediate surroundings with large shifts in excitation and emission peaks (Cohen et al., 2002), making them ideal for reporting protein allostery, particularly in proteins with domains moving in and out of membranes (Cohen et al., 2005; Fletcher-Taylor et al., 2020). Both excitation and emission typically move to longer wavelengths as surroundings become more polar (i.e., solvatochromic shifts). Ligands conjugated to these fluorophores are conformation sensitive if the local environment (e.g., lipid, protein, or aqueous) of the conjugated probe is altered during activity, enabling monitoring of structural changes in real time. Local changes in protein structure may be resolved on femtosecond to second timescales (Abbyad et al., 2007) and measured in conjunction with live-cell electrophysiological recording (Cohen et al., 2005; Fletcher-Taylor et al., 2020).

One such family of Kv2 EVAP have been synthesized to contain julolidine phenoxazone (JP), a far red environment-sensitive fluorophore with large spectral shifts useful for live-cell imaging (Fletcher-Taylor et al. 2020). This EVAP is capable of measuring conformational changes that

are consistent with measurements of electronic gating currents (Fig 5). With one GxTX conjugate in which a reactive propargylglycine (Pra) is substituted for a Lys and conjugated to JP, Lys27Pra(JP), the emission shift midpoint is 50 mV more negative than the Kv2.1 gating current midpoint (Fig 5 C) or subsequent channel opening. This suggests that the conformational changes that alter the immediate environment of the JP are early VSD motions in the closed channel and are not concerted with VSD motions at more depolarized potentials. Careful studies of Kv gating currents have shown distinct early and late VSD conformational changes as the membrane is stepped to more positive voltages (Fletcher-Taylor et al., 2020). One structural hypothesis of VSD allostery is that negatively charged Kv residues residing in the center of the membrane electric field stabilize distinct S4 conformations in the transition from resting to active states (Schoppa & Sigworth, 1998; Zagotta et al., 1994). Coupled with high-resolution structures of channels complexed with different gating modifier toxins as well as structures of channels in multiple states (Shen et al., 2019; Wisedchaisri et al., 2021; Xu et al., 2019), EVAPs will enable predictions and improved models of channel allostery. Other types of Kv EVAPs include those conjugated to semiconductor quantum dots (Mann et al., 2018), whose sensitivity to electric fields may make them useful as single-molecule voltage sensors.

[Insert Figure 5 here]

3. Endogenous Voltage-Sensor Activation Probe Synthesis and Imaging

EVAP imaging is compatible with live cell and tissue fluorescence imaging. The method of microscopy used will depend on the needs of specific experiments. The EVAPs described here are compatible with many fluorescence microscopes. For any hypothesis that is tested with EVAPs, a validation of the methods should be conducted in your own laboratory. The protocol we present below is specifically for synthesis of GxTX-based EVAPs and imaging with Kv2.1 channels expressed in CHO-K1 cells, that could serve as in-house validation of the EVAPs described. While we do our own synthesis, the EVAP synthesis could be carried out by a peptide synthesis company.

3.1 Equipment

1. *Peptide-fluorophore conjugation*

- Semi-preparatory or preparatory HPLC with C18 column for peptides

- Lyophilizer compatible with acetonitrile and trifluoracetic acid

- MALDI-TOF Mass spectrometer

- UV/Vis spectrophotometer

2. *Imaging*

- Fluorescence imaging microscope for live cells or tissue. We have used wide field, 2-photon excitation, TIRF and confocal. As fluorescence signal can be limited by photobleaching over the course of an experiment, give special consideration as to what

fraction of emitted fluorophores are captured by the microscope; confocal microscopy can be disadvantageous because photons emitted outside of the focal spot are discarded. For environment-sensitive EVAPs a means of distinguishing emission wavelengths is needed. This can either be multiple emission filters, or a spectral imaging microscope. Several commercial varieties of scanning confocal microscopes are available that measure point-by-point emission spectra.

3. Electrophysiology

- Patch clamp amplifier

4. Protocols

4.1 Design of a peptide toxin – fluorophore conjugate

1. *Choose a fluorescence labeling strategy*

We have found that a key to success in labeling cystine knot peptides is inserting a small reactive side chain that can be conjugated to fluorophores by high-yield click chemistry. For example, the synthetic amino acid propargylglycine (Pra) can be substituted into a peptide variant and conjugated to azide-functionalized fluorescent dyes (Fletcher-Taylor et al., 2020). A cysteine residue orthogonally protected (e.g., with an acetaminomethyl group, Cys(Acm)), can be deprotected following refolding and labeled with a maleimide-functionalized fluorescent dye (Tilley et al., 2014). Fluorescent amino acids and larger side chains have tended to interfere with formation of disulfide bridges during the folding process.

A wide variety of maleimide- or azide-functionalized fluorophores are amenable to EVAP conjugation. For a dynamic studies, hydrophilic fluorophores are preferable as they reduce non-specific membrane partitioning, decreasing background signal. Many commercial fluorophores are charged and connected to protein-conjugation groups via linkers, which increase the solubility of the peptide-fluorophore conjugate and may prevent the fluorophore from interfering with binding to the channel. For these studies, commercial fluorophores Dylight 550, DyLight 633, and Alexa Fluor 594 have enabled imaging of channel activity (Tilley et al., 2014; Thapa et al., 2021). For environment-sensitive studies, we have described a lipophilic fluorophore, julolidine phenoxazone azide, JP-N$_3$, which can improve GxTX affinity for Kv2.1 if properly positioned (Fletcher-Taylor et al., 2020). New fluorophores that can be imaged into the near infrared would enable deep tissue imaging and multiplexed EVAP sensing.

2. *Choose a residue on a conformation-selective peptide toxin to use as a point of chemoselective conjugation by fluorophores*

For dynamic EVAPs, we aim for a position away from the peptide–protein binding interface, which is expected to be exposed to the extracellular solution. Comparing peptide toxin sequences and identifying highly variable residues can be helpful in choosing a site that is not critical to peptide function. For a dynamic GxTX EVAP, replacing Ser13 with Cys(Acm) or Pra works well. For an environment-sensitive EVAP, a site near where large changes in the chemical environment occur during conformational change is most important, but will invariably lead to more conjugates that do not bind to the channel. For GxTX we replace Lys27 with Cys(Acm). For stability and ease of synthesis, replacement of Met residues with isosteric norleucine (Nle) residues prevents loss of peptide by Met oxidation, especially during oxidative refolding.

4.2 Oxidative folding of peptide toxin variants

Reagents

lyophilized, reduced linear GxTX peptide with a chemoselective conjugation site

  e.g., GxTX Ser13Cys(Acm) Met35Nle or GxTX Lys27Pra Met35Nle

guanidinium hydrochloride

ammonium acetate

glutathione

oxidized glutathione

acetonitrile

ammonium hydroxide

trifluoroacetic acid

1. Dissolve the linear, reduced peptide in 50% acetonitrile, and then dilute to 50 μM in oxidation buffer at 4° C (1 M guanidinium hydrochloride, 0.1 M ammonium acetate, 2.5 mM glutathione, 0.25 mM oxidized glutathione, and 1% acetonitrile, adjusted to pH 8.0 with ammonium hydroxide).

2. Stir vigorously at 4° C to oxygenate the solution. Monitor disulfide formation as proton loss by mass spectrometry. For GxTX variants, complete oxidative folding requires approximately three days.

3. When oxidation is complete, purify the folded peptide toxin variant by HPLC. Filter the solution, add acetonitrile to 20%, trifluoroacetic acid to 0.1% and pump directly onto the HPLC column. Solvent A = 0.1% trifluoroacetic acid in water. Solvent B = 0.1% trifluoroacetic acid in acetonitrile. Pump at 30% B until flowthrough absorbance stabilizes then slowly increase % B at 0.25% per minute. Peptide should elute at about 35% B. Folding will typically shift retention time on the HPLC. The properly-folded peptide toxin will often be the first major peak to be eluted from the column.

4. Lyophilize folded peptide toxins and store with desiccant at -20° C. Note that electrostatic phenomena can lead to inaccuracy when weighing fluffy peptide lyophilizates. Determining concentration from a calculated 280 nm extinction coefficient may be more accurate.

4.3 Conjugation to azide-fluorophore

This protocol is specifically for generation of the GxTX Lys27Pra(JP) EVAP (Fletcher-Taylor et al., 2020). This is by conjugation of GxTX with a propargylglycine at position 27 to julolidine phenoxazone azide (JP-N$_3$) via Cu(I)-catalyzed azide-alkyne click cycloaddition.

Reagents

GxTX Lys27Pra Met35Nle, or other alkyne functionalized, folded peptide toxin

JP-N$_3$, or other azide-fluorophore

BTTAA, bis[(tertbutyltriazoyl)methyl]-[(2-carboxymethyltriazoyl)methyl] -amine (Besanceney-Webler et al., 2011)

CuSO$_4$ copper sulfate

DMSO, dimethyl sulfoxide

sodium ascorbate

ascorbic acid

EDTA, ethylenediaminetetraacetic acid

arginine hydrochloride

glutamate

sodium hydroxide

1. To a polypropylene tube sequentially add: 24 µL of a premixed aqueous solution containing 2.5 mM CuSO$_4$ (60 nmol) with 15 mM BTTAA (360 nmol); followed by 30 µL of 1 mM JP-N3 (30 nmol) in DMSO, 42 µL of DMSO, and 8 µL of 1.9 mM GxTX Lys27Pra (15 nmol); 10 µL of 150 mM freshly mixed 10:1 sodium ascorbate:ascorbic acid (1.5 µmol).

2. Briefly vortex the reaction mixture after each addition.

3. Shake the reaction in the dark at 25 °C for 4 h before quenching with 10 μL of 50 mM EDTA, pH 5.

4. Purify by HPLC.

5. Lyophilize and store dessicated at -20° C.

Note: Lyophilized EVAP conjugates can be difficult to dissolve in solution. Sonication can accelerate this solvation process. We use arginine as an excipient to improve EVAP solubility (1 M arginine hydrochloride, 50 mM glutamate, pH 5.0 with sodium hydroxide), and store in aliquots at -80 °C.

4.4 Deprotection of spinster cysteine and conjugation to maleimide-fluorophore

This protocol is specifically for generation of the GxTX-594 EVAP (Thapa et al., 2021). This is done by conjugation of GxTX with a cysteine at position 13 to Alexa Fluor 594 via a thiol-maleimide linkage.

Reagents

GxTX Ser13Cys(Acm) Met35Nle, or other folded peptide toxin functionalized with Cys(Acm)

Alexa Fluor 594 C_5 maleimide, or other maleimide-fluorophore

trifluoroacetic acid

anisole

silver acetate

diethyl ether

acetic acid

guanidinium hydrochloride

acetonitrile

disodium EDTA

Tris, tris(hydroxymethyl)aminomethane

DMSO

hydrochloric acid

Deprotection of Cys(Acm)

1. Dissolve peptide with Cys(Acm) in trifluoroacetic acid + 1% anisole to a final concentration of 10 mg/mL (2.5 mM).

2. Add silver acetate to 30 mg/mL (0.18 M) and mix with slow rotation while protected from light. Monitor deprotection by mass spectrometry. Acm deprotection requires approximately 2 hours.

3. Pellet peptide with diethyl ether.

4. Remove the remaining silver by dissolving the pellet in 50% acetic acid and adding a 1 volume of 2 M guanidinium hydrochloride while incubating for 10 minutes at room temperature.

5. Purify deprotected Cys peptide by HPLC and lyophilize.

Conjugation of Cys peptide to maleimide-fluorophore

6. Bring lyophilisate of Cys peptide substitution to 300 µM in 50% (vol/vol) acetonitrile + 1

mM disodium EDTA. Mix this solution with one part 200 mM Tris, 20 mM disodium

EDTA (pH 6.8 with hydrochloric acid).

7. Add a 2.5-mM solution of the maleimido–fluorophore in DMSO to 20% (vol/vol) final

DMSO concentration.

8. Agitate in a polypropylene tube for 2 h at 20 °C.

9. Purify by HPLC as described above.

4.5 Voltage Clamp Fluorescence Imaging

To image conformational changes of ion channels with EVAPs, you will need an imaging system

with an incorporated method for stimulating the targeted ion channel's voltage sensors. The most

controlled way to elicit conformational change to test or calibrate an EVAP is voltage clamp of a

cell expressing its target ion channels. This protocol describes our methods for effectively

voltage clamping cells and imaging EVAP responses with GxTX-fluorophores.

Supplies and Solutions

Amounts required for a single plate of cells are listed.

1. Ion channel preparation in live cells.

   e.g. CHO-K1 cells expressing Kv2.1 channels, plated in a 35 mm dish with a 7 mm

   glass center.

2. Extracellular solution appropriate for live cell preparation. Sufficient volume to rinse

   cells.

   10 mL of (in mM): 3.5 KCl, 155 NaCl, 10 HEPES, 1.5 $CaCl_2$, 1 $MgCl_2$, 10 glucose

   adjusted to pH 7.4 with NaOH. Measured osmolarity is 315 mOsm for this solution.

If patch-clamping is not being conducted, 1% BSA (bovine serum albumin, Fraction V, protease free) can be included in extracellular solution, to minimize peptide adsorption to surfaces. Care should be taken to avoid frothing BSA solutions.

3. EVAP solution: Sufficient volume of appropriate EVAP solution to apply to cells. e.g. 1 mL of 100 nM GxTX-fluorophore.

4. Intracellular pipette solution

   1 mL of (in mM): 70 mM CsCl, 50 mM CsF, 35 mM NaCl, 1 mM EGTA, 10 mM HEPES, brought to pH 7.4 with CsOH. Osmolarity is adjusted to 310 mOsm.

5. Pipette glass

Protocol

1. Wash CHO cells plated on glass-bottom dish 3x with extracellular solution.

2. Replace extracellular solution with a minimal volume EVAP solution. The appropriate concentration will depend on the hypothesis that is being tested. Concentrations above the K_d of GxTX-594 for the resting voltage sensor conformation will label most Kv2 proteins. Concentrations well below this K_d will inhibit fewer channels and have lower signal to noise. The time of incubation in GxTX-594 will also depend on the concentration used. Watch for labeling equilibration to determine the incubation time required. We found that at a concentration of 100 nM GxTX-594, fluorescence equilibrates on CHO cells in approximately 5 minutes or into brain slices in 10 minutes (Thapa et al., 2021).

3. Collect fluorescence images. One of the biggest limitations with EVAP imaging (and imaging of any membrane fluorescence) is photobleaching. Care should be taken to

minimize photobleaching. Maximizing photon capture is also important. On a confocal microscope a trade-off between resolution and photobleaching can be made by opening up the microscope's pinhole, which reduces resolution but increases the photons captured by the PMT.

4. Voltage clamp cells. Pull borosilicate glass pipettes with blunt tips, less than 3.0 MΩ. To limit current-induced voltage error, patch pipette can contain solution to block channels. For K$^+$ channel EVAPs we use a K$^+$-deficient Cs$^+$ internal solution. Voltage-clamp a cell with obvious GxTX surface staining in whole-cell mode. Monitor currents and series resistance throughout the experiment to assess series resistance-induced voltage clamp error.

Note: Internalization of the Kv2.1-GxTX-594 complex occurs on the timescale of imaging experiments and can alter voltage clamp fluorometry measurements. Complete all experiments as soon as possible after application of EVAP, as internalization of membrane proteins could remove fluorophores from the surface membrane. We have noted significant apparent internalization an hour after GxTX-594 is added, consistent with studies of Kv2.1 endocytosis (Thapa et al., 2021).

5. Analysis

5.1 Dynamic fluorescence

To enable translation of the intensity of fluorescence from a dynamic EVAP on a cell surface into a measure of conformational change, we developed a series of equations derived from rate theory that relate cell labeling to voltage sensor activation, which we refer to as the EVAP Model (Thapa et al., 2021). Predictions of the EVAP Model with the kinetic parameters of the GxTX-594–Kv2.1 interaction are represented in Figure 6. In the GxTX EVAP model, the proportion of labeled vs. unlabeled Kv2 in a membrane is determined by the proportion of voltage sensors in resting vs. activated conformations. When voltage sensors change from resting to activated conformations, the binding rate of the GxTX-594 EVAP decreases and the unbinding rate increases. When the membrane voltage is held constant for sufficient time, the proportions of labeled and unlabeled proteins reach an equilibrium. The EVAP model predicts that as GxTX-594 concentration decreases, the change in labeling ($\Delta F/\Delta F_{max}$) asymptotically approaches the probability that unlabeled voltage sensors are resting (Fig 6). Thus, the thermodynamics of the free EVAP, labeled and unlabeled Kv2 proteins reduce to a simple interpretation: a decrease in GxTX-594 fluorescence indicates a decrease in the fraction of unlabeled voltage sensors that are in resting conformations.

[Insert Figure 6 here]

To investigate the relationship between voltage sensor conformational change and conformation dependent EVAP fluorescence, both the amplitude and kinetics of fluorescence change from cell surface Regions Of Interest (ROIs) can be analyzed and interpreted via the EVAP model.

To determine the rate of florescence change ($k_{\Delta F}$) of EVAPs, the change in fluorescence intensity can be fit with a monoexponential function:

$$F = F_\infty + (F_0 - F_\infty)\, e^{-\frac{(t-t_0)}{\tau}}$$

Where $\tau = 1/k_{\Delta F}$, t = time, t_0 = time at start of fit, F = fluorescence intensity, F_0 = fluorescence at start of fit, F_∞ = fluorescence after infinite time (Figs 1,2,3).

5.2 Environment-sensitive fluorescence

To analyze the voltage-dependent changes in structure reported by environment-sensing EVAPs, fluorescence emissions at multiple wavelengths are compared. To determine the voltage-dependent changes in the GxTX-VSD structure, we measured full emission spectra from Lys27Pra(JP). Raw emission data can be fit with split pseudo-Voigt functions, with 2-component fits being more accurate than single component fits or other lineshape functions.

To fit with split pseudo-Voigt functions, fluorescence emission spectra are decomposed into one or more 6-parameter split pseudo-Voigt curves (Thapa et al., 2021) expressed as an inequality with the form:

$$y(x; a_0, a_1, a_2, a_3, a_4, a_5) = \begin{cases} PseudoVoigt(x; a_0, a_1, a_2, a_4) & x \le a_1 \\ PseudoVoigt(x; a_0, a_1, a_3, a_5) & x > a_1 \end{cases}$$

where a_0 is the amplitude, a_1 is the midpoint, and a_2-a_5 are shape definition parameters. The 4-parameter pseudo-Voigt function in each range is in the form:

$$y = a_0 \left[(1 - a_3)\exp\left(-\ln(2)\left(\frac{x - a_1}{a_2}\right)^2 \right) + \frac{a_3}{1 + \left(\frac{x - a_1}{a_2}\right)^2} \right]$$

In unconstrained fittings, all parameters (a_0-a_5) are optimized during fitting. Otherwise, only a_0 and a_1 are optimized, while a_2-a_5 are constrained to a reference spectrum. In the case of a Lys27Pra(JP) GxTX on Kv2.1-expressing cells, a split pseudo-Voigt fit at -80 mV membrane potential can serve as a reference spectrum (Fig. 5A). We have also described further details and options for fitting methods (Adhikary et al., 2014; Aschaffenburg & Moog, 2009; Greathouse et al., 2007; Jha et al., 2012).

We show our findings with this EVAP as an example of analysis. When analyzing the EVAP GxTX Lys27Pra(JP), fit functions consistently show non-polar (~610 nm) and polar (~640 nm) peaks, with gradual increases in the polar component as the VSD moves from its resting to activated state (Fig 5). This suggests multiple JP-GxTX-VSD species are present, and that depolarization changes the dominant JP species from a lipid/protein environment to a more polar one. The 2-component fits are optimal lineshapes for the data but do not necessarily mean there are exactly 2 species, or that the weightings of the fit components reflect percentages of particular conformations. However, mean emission spectra calculated from integrations of 2-component fittings show a redshift fit well by a two-state Boltzmann function with a midpoint ($F_{1/2}$) of -15 mV, and that plateaus above +40 mV (Fig 5 C). By comparison, gating currents (Q_{off}) of the Kv2.1-Lys27Pra(JP) GxTX complex, which reflect the activation of S4 and movement of its 3 Arg through the membrane electric field, have a midpoint of +36 mV. At the $F_{1/2}$ of -15 mV, Q_{off} is at ~5% of its maximal value. This large discrepancy between voltage-dependent fluorescence shifts and gating currents suggests VSD allostery closest to GxTX Lys27 is distinct from the majority of S4 structural changes, reflecting either unconcerted motions within S4, fast relaxation to other conformations, or other complexities

not typically considered in models of channel allostery.

6. Summary

The EVAP methods of using fluorescent toxins as activity sensors enables measurement of voltage-sensitive conformational changes of a specific subtype of endogenous ion channel. Imaging EVAP fluorescence reveals conformational changes in ion channels with subcellular spatial resolution, offering new dimensions of molecular and spatial information to complement research with temporally precise electrophysiological techniques. The same principles of EVAP action could apply to many other conformation-selective labeling reagents, suggesting that probes for conformational changes of many different proteins could be developed.

Acknowledgments

References

Abbyad, P., Shi, X., Childs, W., McAnaney, T. B., Cohen, B. E., & Boxer, S. G. (2007).
Measurement of solvation responses at multiple sites in a globular protein. *The Journal of
Physical Chemistry. B*, *111*(28), 8269–8276. https://doi.org/10.1021/jp0709104

Adams, S. R. (2010). How calcium indicators work. *Cold Spring Harbor Protocols*, *2010*(3),
pdb.top70. https://doi.org/10.1101/pdb.top70

Adhikary, R., Zimmermann, J., Dawson, P. E., & Romesberg, F. E. (2014). IR probes of protein
microenvironments: utility and potential for perturbation. *Chemphyschem : A European
Journal of Chemical Physics and Physical Chemistry*, *15*(5), 849–853.
https://doi.org/10.1002/cphc.201400017

Aggarwal, S. K., & MacKinnon, R. (1996). Contribution of the S4 segment to gating charge in
the Shaker K+ channel. *Neuron*, *16*(6), 1169–1177. https://doi.org/10.1016/s0896-
6273(00)80143-9

Ahuja, S., Mukund, S., Deng, L., Khakh, K., Chang, E., Ho, H., Shriver, S., Young, C., Lin, S.,
Johnson, J. P. J., Wu, P., Li, J., Coons, M., Tam, C., Brillantes, B., Sampang, H., Mortara,
K., Bowman, K. K., Clark, K. R., … Payandeh, J. (2015). Structural basis of Nav1.7
inhibition by an isoform-selective small-molecule antagonist. *Science (New York, N.Y.)*,
350(6267), aac5464. https://doi.org/10.1126/science.aac5464

Armstrong, C. M., & Bezanilla, F. (1973). Currents related to movement of the gating particles
of the sodium channels. *Nature*, *242*(5398), 459–461. https://doi.org/10.1038/242459a0

Aschaffenburg, D. J., & Moog, R. S. (2009). Probing hydrogen bonding environments:
solvatochromic effects on the CN vibration of benzonitrile. *The Journal of Physical*

Chemistry. B, *113*(38), 12736–12743. https://doi.org/10.1021/jp905802a

Besanceney-Webler, C., Jiang, H., Zheng, T., Feng, L., Soriano del Amo, D., Wang, W., Klivansky, L. M., Marlow, F. L., Liu, Y., & Wu, P. (2011). Increasing the efficacy of bioorthogonal click reactions for bioconjugation: a comparative study. *Angewandte Chemie (International Ed. in English)*, *50*(35), 8051–8056. https://doi.org/10.1002/anie.201101817

Catterall, W. A., Cestèle, S., Yarov-Yarovoy, V., Yu, F. H., Konoki, K., & Scheuer, T. (2007). Voltage-gated ion channels and gating modifier toxins. *Toxicon : Official Journal of the International Society on Toxinology*, *49*(2), 124–141. https://doi.org/10.1016/j.toxicon.2006.09.022

Cohen, B. E., McAnaney, T. B., Park, E. S., Jan, Y. N., Boxer, S. G., & Jan, L. Y. (2002). Probing protein electrostatics with a synthetic fluorescent amino acid. *Science (New York, N.Y.)*, *296*(5573), 1700–1703. https://doi.org/10.1126/science.1069346

Cohen, B. E., Pralle, A., Yao, X., Swaminath, G., Gandhi, C. S., Jan, Y. N., Kobilka, B. K., Isacoff, E. Y., & Jan, L. Y. (2005). A fluorescent probe designed for studying protein conformational change. *Proceedings of the National Academy of Sciences of the United States of America*, *102*(4), 965–970. https://doi.org/10.1073/pnas.0409469102

Dockendorff, C., Gandhi, D. M., Kimball, I. H., Eum, K. S., Rusinova, R., Ingólfsson, H. I., Kapoor, R., Peyear, T., Dodge, M. W., Martin, S. F., Aldrich, R. W., Andersen, O. S., & Sack, J. T. (2018). Synthetic Analogues of the Snail Toxin 6-Bromo-2-mercaptotryptamine Dimer (BrMT) Reveal That Lipid Bilayer Perturbation Does Not Underlie Its Modulation of Voltage-Gated Potassium Channels. *Biochemistry*, *57*(18), 2733–2743. https://doi.org/10.1021/acs.biochem.8b00292

Du, J., Tao-Cheng, J. H., Zerfas, P., & McBain, C. J. (1998). The K+ channel, Kv2.1, is apposed

to astrocytic processes and is associated with inhibitory postsynaptic membranes in hippocampal and cortical principal neurons and inhibitory interneurons. *Neuroscience*, *84*(1), 37–48. https://doi.org/10.1016/s0306-4522(97)00519-8

Fletcher-Taylor, S., Thapa, P., Sepela, R. J., Kaakati, R., Yarov-Yarovoy, V., Sack, J. T., & Cohen, B. E. (2020). Distinguishing Potassium Channel Resting State Conformations in Live Cells with Environment-Sensitive Fluorescence. *ACS Chemical Neuroscience*, *11*(15), 2316–2326. https://doi.org/10.1021/acschemneuro.0c00276

Greathouse, J. A., Cygan, R. T., Bradshaw, R. W., Majzoub, E. H., & Simmons, B. A. (2007). Computational and Spectroscopic Studies of Dichlorofluoroethane Hydrate Structure and Stability. *The Journal of Physical Chemistry C*, *111*(45), 16787–16795. https://doi.org/10.1021/jp072968o

Herrington, J., Zhou, Y.-P., Bugianesi, R. M., Dulski, P. M., Feng, Y., Warren, V. A., Smith, M. M., Kohler, M. G., Garsky, V. M., Sanchez, M., Wagner, M., Raphaelli, K., Banerjee, P., Ahaghotu, C., Wunderler, D., Priest, B. T., Mehl, J. T., Garcia, M. L., McManus, O. B., … Slaughter, R. S. (2006). Blockers of the delayed-rectifier potassium current in pancreatic beta-cells enhance glucose-dependent insulin secretion. *Diabetes*, *55*(4), 1034–1042. https://doi.org/10.2337/diabetes.55.04.06.db05-0788

Islas, L. D., & Sigworth, F. J. (1999). Voltage sensitivity and gating charge in Shaker and Shab family potassium channels. *The Journal of General Physiology*, *114*(5), 723–742. https://doi.org/10.1085/jgp.114.5.723

Jha, S. K., Ji, M., Gaffney, K. J., & Boxer, S. G. (2012). Site-specific measurement of water dynamics in the substrate pocket of ketosteroid isomerase using time-resolved vibrational spectroscopy. *The Journal of Physical Chemistry. B*, *116*(37), 11414–11421.

https://doi.org/10.1021/jp305225r

Lewis, G. N. (1925). A New Principle of Equilibrium. *Proceedings of the National Academy of Sciences of the United States of America*, *11*(3), 179–183. https://doi.org/10.1073/pnas.11.3.179

Long, S. B., Campbell, E. B., & Mackinnon, R. (2005). Voltage sensor of Kv1.2: structural basis of electromechanical coupling. *Science (New York, N.Y.)*, *309*(5736), 903–908. https://doi.org/10.1126/science.1116270

Long, S. B., Tao, X., Campbell, E. B., & MacKinnon, R. (2007). Atomic structure of a voltage-dependent K+ channel in a lipid membrane-like environment. *Nature*, *450*(7168), 376–382. https://doi.org/10.1038/nature06265

Mann, V. R., Powers, A. S., Tilley, D. C., Sack, J. T., & Cohen, B. E. (2018). Azide-Alkyne Click Conjugation on Quantum Dots by Selective Copper Coordination. *ACS Nano*, *12*(5), 4469–4477. https://doi.org/10.1021/acsnano.8b00575

McCormack, K., Santos, S., Chapman, M. L., Krafte, D. S., Marron, B. E., West, C. W., Krambis, M. J., Antonio, B. M., Zellmer, S. G., Printzenhoff, D., Padilla, K. M., Lin, Z., Wagoner, P. K., Swain, N. A., Stupple, P. A., de Groot, M., Butt, R. P., & Castle, N. A. (2013). Voltage sensor interaction site for selective small molecule inhibitors of voltage-gated sodium channels. *Proceedings of the National Academy of Sciences of the United States of America*, *110*(29), E2724-32. https://doi.org/10.1073/pnas.1220844110

McDonough, S. I., Mintz, I. M., & Bean, B. P. (1997). Alteration of P-type calcium channel gating by the spider toxin omega-Aga-IVA. *Biophysical Journal*, *72*(5), 2117–2128. https://doi.org/10.1016/S0006-3495(97)78854-4

Peretz, A., Pell, L., Gofman, Y., Haitin, Y., Shamgar, L., Patrich, E., Kornilov, P., Gourgy-

Hacohen, O., Ben-Tal, N., & Attali, B. (2010). Targeting the voltage sensor of Kv7.2 voltage-gated K+ channels with a new gating-modifier. *Proceedings of the National Academy of Sciences of the United States of America*, *107*(35), 15637–15642. https://doi.org/10.1073/pnas.0911294107

Sack, J. T., Aldrich, R. W., & Gilly, W. F. (2004). A gastropod toxin selectively slows early transitions in the Shaker K channel's activation pathway. *The Journal of General Physiology*, *123*(6), 685–696. https://doi.org/10.1085/jgp.200409047

Schmalhofer, W. A., Calhoun, J., Burrows, R., Bailey, T., Kohler, M. G., Weinglass, A. B., Kaczorowski, G. J., Garcia, M. L., Koltzenburg, M., & Priest, B. T. (2008). ProTx-II, a selective inhibitor of NaV1.7 sodium channels, blocks action potential propagation in nociceptors. *Molecular Pharmacology*, *74*(5), 1476–1484. https://doi.org/10.1124/mol.108.047670

Schoppa, N. E., & Sigworth, F. J. (1998). Activation of shaker potassium channels. I. Characterization of voltage-dependent transitions. *The Journal of General Physiology*, *111*(2), 271–294. https://doi.org/10.1085/jgp.111.2.271

Seoh, S. A., Sigg, D., Papazian, D. M., & Bezanilla, F. (1996). Voltage-sensing residues in the S2 and S4 segments of the Shaker K+ channel. *Neuron*, *16*(6), 1159–1167. https://doi.org/10.1016/s0896-6273(00)80142-7

Shen, H., Liu, D., Wu, K., Lei, J., & Yan, N. (2019). Structures of human Na(v)1.7 channel in complex with auxiliary subunits and animal toxins. *Science (New York, N.Y.)*, *363*(6433), 1303–1308. https://doi.org/10.1126/science.aaw2493

Swartz, K. J. (2007). Tarantula toxins interacting with voltage sensors in potassium channels. *Toxicon : Official Journal of the International Society on Toxinology*, *49*(2), 213–230.

https://doi.org/10.1016/j.toxicon.2006.09.024

Tao, X., Lee, A., Limapichat, W., Dougherty, D. A., & MacKinnon, R. (2010). A gating charge transfer center in voltage sensors. *Science (New York, N.Y.)*, *328*(5974), 67–73. https://doi.org/10.1126/science.1185954

Thapa, P., Stewart, R., Sepela, R. J., Vivas, O., Parajuli, L. K., Lillya, M., Fletcher-Taylor, S., Cohen, B. E., Zito, K., & Sack, J. T. (2021). Optical measurement of voltage sensing by endogenous ion channels. *BioRxiv*, 541805. https://doi.org/10.1101/541805

Tilley, D. C., Angueyra, J. M., Eum, K. S., Kim, H., Chao, L. H., Peng, A. W., & Sack, J. T. (2019). The tarantula toxin GxTx detains K(+) channel gating charges in their resting conformation. *The Journal of General Physiology*, *151*(3), 292–315. https://doi.org/10.1085/jgp.201812213

Tilley, D. C., Eum, K. S., Fletcher-Taylor, S., Austin, D. C., Dupré, C., Patrón, L. A., Garcia, R. L., Lam, K., Yarov-Yarovoy, V., Cohen, B. E., & Sack, J. T. (2014). Chemoselective tarantula toxins report voltage activation of wild-type ion channels in live cells. *Proceedings of the National Academy of Sciences of the United States of America*, *111*(44), E4789-96. https://doi.org/10.1073/pnas.1406876111

Turner, M., Anderson, D. E., Bartels, P., Nieves-Cintron, M., Coleman, A. M., Henderson, P. B., Man, K. N. M., Tseng, P.-Y., Yarov-Yarovoy, V., Bers, D. M., Navedo, M. F., Horne, M. C., Ames, J. B., & Hell, J. W. (2020). α-Actinin-1 promotes activity of the L-type Ca(2+) channel Ca(v) 1.2. *The EMBO Journal*, *39*(5), e102622. https://doi.org/10.15252/embj.2019102622

Wisedchaisri, G., Tonggu, L., Gamal El-Din, T. M., McCord, E., Zheng, N., & Catterall, W. A. (2021). Structural Basis for High-Affinity Trapping of the Na(V)1.7 Channel in Its Resting

State by Tarantula Toxin. *Molecular Cell*, *81*(1), 38-48.e4.

   https://doi.org/10.1016/j.molcel.2020.10.039

Xu, H., Li, T., Rohou, A., Arthur, C. P., Tzakoniati, F., Wong, E., Estevez, A., Kugel, C.,

   Franke, Y., Chen, J., Ciferri, C., Hackos, D. H., Koth, C. M., & Payandeh, J. (2019).

   Structural Basis of Nav1.7 Inhibition by a Gating-Modifier Spider Toxin. In *Cell* (Vol. 176,

   Issue 5, pp. 1238–1239). https://doi.org/10.1016/j.cell.2019.01.047

Yang, W., & Yuste, R. (2017). In vivo imaging of neural activity. *Nature Methods*, *14*(4), 349–

   359. https://doi.org/10.1038/nmeth.4230

Zagotta, W. N., Hoshi, T., Dittman, J., & Aldrich, R. W. (1994). Shaker potassium channel

   gating. II: Transitions in the activation pathway. *The Journal of General Physiology*,

   103(2), 279–319. https://doi.org/10.1085/jgp.103.2.279

Zhang, A. H., Sharma, G., Undheim, E. A. B., Jia, X., & Mobli, M. (2018). A complicated

   complex: Ion channels, voltage sensing, cell membranes and peptide inhibitors.

   Neuroscience Letters, *679*, 35–47. https://doi.org/10.1016/j.neulet.2018.04.030

Figure Legends

Figure 1: *EVAP labeling of ion channels in brain slice.*

Structural models and activity of GxTX with Kv channels.

A. Top view of a model of GxTX (green) bound to a Kv2.1 voltage sensor (gold) in its active state. 4 positions of fluorophore conjugation are highlighted. Membrane is shown as hydrophobic interior (yellow) and polar interface (blue),.

B. Side view of the model shown in A.

C. 2-photon excitation images of GxTX-594 labeling of a rat CA1 hippocampal pyramidal neuron in brain slice six days after transfection with Kv2.1-GFP. Kv2.1-GFP (Left), GxTX-594 (Middle) and overlay (Right). Scale bars 10 µm. Endogenous Kv2 channels are labeled on neuron on left side of panels.

Adapted from (Fletcher-Taylor et al., 2020).

Figure 2: *Dynamic EVAP response to voltage stimulus*

A. Solid black line represents fluorescence of voltage-clamped cell in 1 nM GxTX-550. Blue bars indicate action-potential-like epochs: 2-ms steps to +40 mV from a holding potential of -80 mV at 100 Hz. Blue lines are monoexponential fits during action-potential-like epochs.

B. Dose–response profile of Kv2.1 inhibition by GxTX-550. Cells were held at a -100 mV holding potential. The 1 nM GxTX-550 concentration used in panel A inhibits only a small minority of channels.

Adapted from (Fletcher-Taylor et al., 2020; Thapa et al., 2021).

Figure 3: Statistical thermodynamics underlie EVAP fluorescence response

Representation of four different possible conformations of EVAP-channel interactions. Horizontal arrows represent voltage sensor equilibria of channels labeled (top) or unlabeled (bottom) by EVAP. Vertical arrows represent on and off rates of EVAP from voltage sensors at rest (left) or active (right).

Adapted from (Thapa et al., 2021).

Figure 4: *EVAP labeling kinetics depend on spatial access*

    A. Time-lapse images of the glass-adhered surface of a voltage-clamped Kv2.1-CHO cell in 9 nM GxTX-594. Pseudocolored images indicate maximal intensities in white. Time index is in the upper left of each panel and membrane potential is indicated in the upper right. Scale bar in lower right of last panel is 10 μm.

    B. Fluorescence image of the glass adhered surface of a voltage-clamped Kv2.1-CHO cell in 9 nM GxTX-594. Gray lines indicate boundaries of ROIs. Scale bar is 10 μm.

    C. Representative traces of GxTX-594 fluorescence intensity response to voltage changes. Red lines are monoexponential fits. Background subtraction was the average intensity of a region that did not contain cells over the time course of the voltage protocol. Each trace was normalized to initial fluorescence intensity before the application of the voltage stimulus.

    Adapted from (Thapa et al., 2021)

Figure 5: *Environment-sensitive EVAP fluorescence changes color to report ion channel activation.*

A. Fluorescence image of a live dissociated rat hippocampal neuron stained with 100 nM Lys27Pra(JP) GxTX. The cell is excited at 561 nm, and its emission isolated around 625 nm. Scale bar is 10 μm.

B. Normalized fluorescence of Lys27Pra(JP) GxTX on CHO cells expressing Kv2.1 channels at -80 mV.

C. Normalized fluorescence of Lys27Pra(JP) GxTX on CHO cells expressing Kv2.1 channels at +40 mV. Data points are mean ± SEM of normalized emission from 4 cells. All spectra are fit with 2-component split pseudo-Voigt functions (black) with individual components (blue, red).

D. Fluorescence shifts and gating currents of Kv2.1 with Lys27Pra(JP) GxTX, recorded from Kv2.1-expressing CHO cells. Mean fluorescence emission of Lys27Pra(JP) as a function of membrane potential (red circles), calculated from integrations of 2-component split pseudo-Voigt fittings of spectral data. Normalized Kv2.1 gating charge (black triangles), with 100 nM Lys27Pra(JP) GxTX, shown as Q/Qmax and measured as Q_{off} from -140 mV. For both plots, data are mean ± SEM (n = 4 cells) and solid lines are two-state Boltzmann functions. Blue dashed lines are mid-point voltages of fluorescence shift (-15 mV) and Q_{off} (+37 mV).

Adapted from (Fletcher-Taylor et al., 2020)

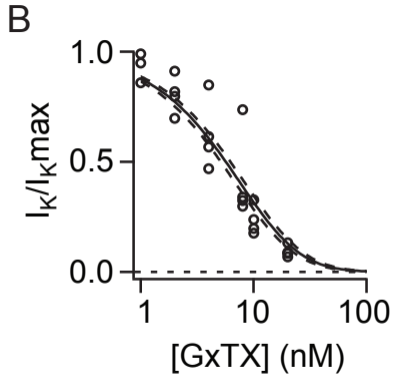**Figure 6:** *Relationship of EVAP labeling to probability of conformational change.*

Outputs of the EVAP Model parameterized for GxTX-594 labeling of Kv2.1 channels.

A. EVAP model predictions of voltage-dependence of cell surface fluorescence intensity at different concentrations of EVAP in solution. Bottom axis represents membrane voltage. The left axis represents the predicted fluorescence relative to the situation where all voltage sensors are at rest and does not include EVAP signal that is insensitive to voltage. The right axis represents the probability that voltage sensors of unlabeled Kv2.1 are in their resting conformation.

B. EVAP model predictions of concentration- and voltage-dependence of $k_{\Delta F}$. Colors correspond to panel A. The right axis represents the probability that voltage sensors of labeled Kv2.1 are in their active conformation.

Adapted From (Fletcher-Taylor et al., 2020)

A

Phe33

Lys10

Lys27

Ser13
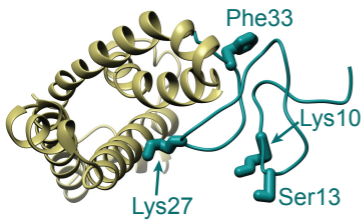
B
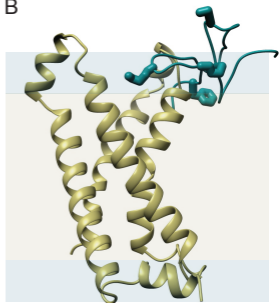
C
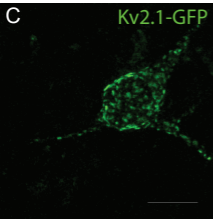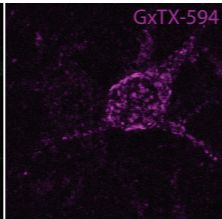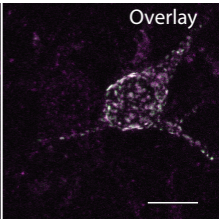
Kv2.1-GFP | GxTX-594 | Overlay
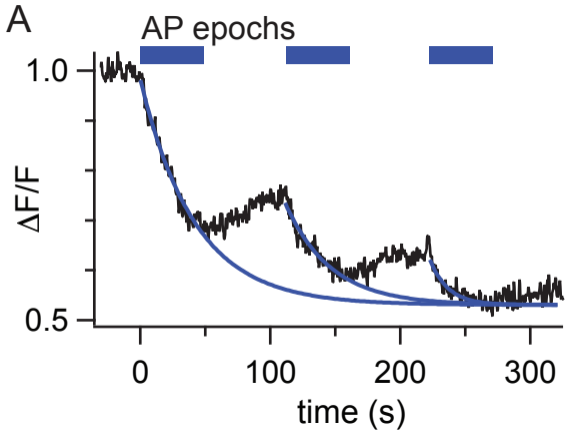
Resting labeled ⇌ Activated labeled

$k_{on,resting} \cdot [EVAP]$ | $k_{off,resting}$ $k_{on,activated} \cdot [EVAP]$ | $k_{off,active}$
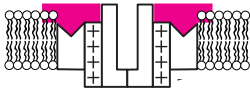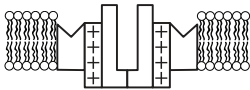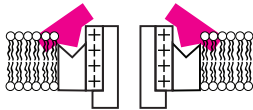
Resting unlabeled ⇌ Activated unlabeled

A 0 s   −80mV 50 s   40mV 130 s   −80mV 540 s   −80mV

B

1
2
3
4

C

40mV
−80mV

F / F_{init}

100%─

40%─

4
3
2
1

0   100   200   300   400   500
Time (s)

A

B

Kv2.1+ cells
$V_m = -80$ mV
$R^2 = 0.996$

C

Kv2.1+ cells
$V_m = +40$ mV
$R^2 = 0.984$

D

A

B